Prepared for submission to JHEP

Phenomenology of the trilinear Higgs coupling at proton-proton colliders

Magdalena Slawinska,[1] **Wouter van den Wollenberg,**[1,2] **Bob van Eijk,**[1] **Stan Bentvelsen**[1,3]

[1] *Nikhef, Science Park 105, 1098 XG, Amsterdam, The Netherlands*
[2] *University of Twente, Drienerlolaan 5, 7522 NB Enschede, The Netherlands*
[3] *University of Amsterdam, Spui 21, 1012 WX Amsterdam, The Netherlands*

Abstract: We investigate Higgs pair production at proton-proton colliders, with emphasis on the gluon fusion channel at the HL-LHC. We study the behaviour of the leading order matrix element using exact computation of quark loops and infinite quark mass approximation. We analyse di-Higgs kinematics in search for phase space regions where the contribution of Higgs self-coupling to SM Higgs pair production is enhanced. We discuss how non-SM values of the Higgs trilinear coupling may affect the kinematics of the Higgs pair.

arXiv:1408.5010v2 [hep-ph] 18 Sep 2014

Contents

1 Introduction 1

2 Higgs pair production through gluon fusion 2

3 Higgs pair differential cross-section 6

4 Disentangling the signal from irreducible background 8

5 Non Standard Model values of λ_{3H} 10

6 Conclusions 13

1 Introduction

Recently, a new scalar boson has been discovered at the Large Hadron Collider at CERN [1, 2]. The scalar has a mass of approximately 125 GeV and decays into fermions and gauge bosons at a rate consistent with the predictions for a Standard Model (SM) Higgs [3, 4]. If the new particle is indeed the SM Higgs boson, it explains electroweak symmetry breaking and completes the particle content of the SM. To understand the dynamics of electroweak symmetry breaking, a detailed measurement of the Higgs potential is indispensable. The SM Higgs mechanism [5, 6] is responsible for generating the mass of electroweak vector bosons via a non-zero vacuum expectation value (VEV) of the Higgs field (ϕ) and restores the unitarity of the theory. The potential of the Higgs field has the form:

$$V(|\phi|^2) = \mu^2|\phi|^2 + \lambda|\phi|^4, \tag{1.1}$$

where $\lambda > 0$ and $\mu^2 < 0$. The dependence on $|\phi|^2$ is motivated by gauge invariance and the polynomial form gives the simplest expression for a renormalisable potential. The minimum value of the Higgs potential is the VEV, $v^2 = -\mu^2/\lambda$. After spontaneous symmetry breaking, $\phi = (v + H^0)/\sqrt{2}$, where H^0 is the excitation from the VEV, the Higgs boson acquires mass $m_H^2 = -2\mu^2 = 2\lambda v^2$, as well as cubic and quartic self-interactions:

$$\begin{aligned} V(H^0) &= 2\lambda v^2 \frac{(H^0)^2}{2} + 6\lambda v \frac{(H^0)^3}{3!} + 6\lambda \frac{(H^0)^4}{4!} - \frac{v^4\lambda}{4} \\ &\equiv m_H^2 \frac{(H^0)^2}{2} + \lambda_{3H} \frac{(H^0)^3}{3!} + \lambda_{4H} \frac{(H^0)^4}{4!} - \frac{v^4\lambda}{4}. \end{aligned} \tag{1.2}$$

The SM Higgs triple and quartic couplings are uniquely defined and read:

$$\lambda_{3H} = \frac{3m_H^2}{v}, \quad \lambda_{4H} = \frac{3m_H^2}{v^2}. \tag{1.3}$$

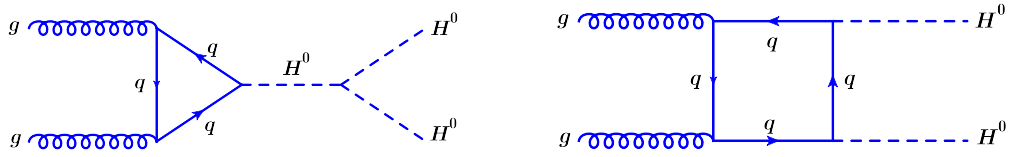

Figure 1. Leading order Feynman diagrams for SM Higgs pair production in gluon-gluon fusion.

In this paper we focus on the triple Higgs coupling λ_{3H}. We review the production of two Higgs bosons in a single collision at hadron colliders and demonstrate that only a fraction of these events is due to processes involving Higgs self-couplings. To determine the size of signal and background, we revisit the mechanisms of Higgs pair production. In section 2 we concentrate on production via gluon-gluon fusion and a quark loop. We compare exact and approximate leading order matrix elements. As the main contribution to the quark loop stems from the top quark, the exact calculation includes the proper (physical) top quark mass while the approximation takes the limit in which the top quark mass becomes infinitely large ('effective field theory' - EFT [7–9]). Next, in section 3, we calculate cross-sections at the LHC and analyse the di-Higgs kinematics. The emphasis is on kinematical properties that may enhance the terms including the trilinear Higgs coupling versus SM Higgs pair production. In Section 4 we discuss potential decay channels for identifying events with Higgs pairs at the HL-LHC and estimate production cross-sections for Higgs pairs at a 100 TeV hadron collider. In Section 5 we compare SM cross-sections with those in which the trilinear Higgs coupling is modified by beyond SM physics.

2 Higgs pair production through gluon fusion

In proton-proton collisions, the most important processes contributing to events with two Higgs bosons in the final state are presented in Table 1. Both leading order (LO) and higher order (NLO and NNLO) cross-sections are listed. The dominant production channel is gluon-gluon fusion, exceeding vector boson fusion by a factor of ∼20. The Higgs pair production channels listed in Table 1 include diagrams for both self-coupling and where two Higgses are produced separately. Quoted errors reflect scale uncertainties only ($\sqrt{\hat{s}}/2 <$ scale $< 2\sqrt{\hat{s}}$). The leading order Feynman diagrams for Higgs pair production in gluon-gluon fusion are shown in Fig. 1. Only the 'triangle' diagram contains the trilinear Higgs coupling. To obtain the di-Higgs cross-section, both diagrams and their interference need to be evaluated.

The expression for the partonic cross-section is given by [10, 14]:

$$\hat{\sigma}^{(LO)}_{gg\to H^0H^0} = \int d\hat{t}\, \frac{\alpha^2\alpha_S^2}{2^{15}\pi M_W^4} \left(|C_\triangle F_\triangle + C_\square F_\square|^2\right), \tag{2.1}$$

where $C_\triangle F_\triangle$ and $C_\square F_\square$ correspond to the individual contributions from the diagrams in Fig. 1. The scale in α_S has been set to the invariant mass of the two incoming partons, $\sqrt{\hat{s}}$.

Process	Order	$\sigma(pp \to H^0H^0)$ [fb]
$gg \to H^0H^0$	LO [10]	$16.5^{+4.6}_{-3.5}$
(gluon-gluon fusion)	NLO [10]	$31.9^{+5.5}_{-4.6}$
	NNLO [11]	$40.2^{+3.2}_{-3.5}$
$qq \to qqH^0H^0$	LO [12]	$1.81^{+0.16}_{-0.14}$
(vector boson fusion)	NLO [13]	$2.01^{+0.03}_{-0.02}$
$qq \to W^{\pm}H^0H^0$	LO [12]	$0.43^{+0.005}_{-0.006}$
(associated production)	NNLO [13]	$0.57^{+0.0006}_{-0.002}$
$qq \to Z^0H^0H^0$	LO [12]	$0.27^{+0.004}_{-0.004}$
(associated production)	NNLO [13]	$0.42^{+0.02}_{-0.02}$

Table 1. Dominant cross sections for SM Higgs pair production at the LHC at $\sqrt{s} = 14$ TeV. The errors account for scale uncertainties only, which in case of associated production with W at NNLO are a factor of 10 smaller than uncertainties due to parton distribution functions.

The Mandelstam variable $\hat{t}$ is defined as:

$$\hat{t} = -\frac{1}{2}\left[\hat{s} - 2m_H^2 - \hat{s}\sqrt{1 - \frac{4m_H^2}{\hat{s}}}\cos\theta,\right], \tag{2.2}$$

where θ is the angle between the two final state Higgs bosons in the centre of mass frame. The term in the matrix element squared (MES)

$$|C_{\triangle}F_{\triangle} + C_{\square}F_{\square}|^2 \tag{2.3}$$

requires the calculation of the form factors $F_{\triangle}$ and $F_{\square}$ stemming from the triangle and box loops. The coefficients $C_{\triangle}$ and $C_{\square}$ express the resonance behaviour of the Higgs propagators. $F_{\triangle}$ and $F_{\square}$ can be calculated either exactly or by applying EFT e.g. in the limit where the top quark mass becomes infinite. To our knowledge the analytical comparison between exact and EFT MES has never been performed for a light Higgs ($m_H = 125$ GeV). We investigate the quality of EFT approximation in the following.

The exact formula for $F_{\triangle}$ in eq. (2.3) is given by [14] and [15]:

$$F_{\triangle} = 2\frac{m_q^2}{\hat{s}}\left[2 + \left(4 - \frac{\hat{s}}{m_q^2}\right)m_q^2 C_{ab}\right] = \tau_q[1 + (1-\tau_q)f(\tau_q)], \tag{2.4}$$

where $\tau_q = \frac{4m_q^2}{\hat{s}}$ and m_q is the mass of the fermion in the loop. We only consider the top quark as the contribution from bottom and lighter quarks is negligible. The function $f(\tau_q)$ stems from the scalar integral, with $C_{ab} = -\frac{2}{\hat{s}} f(\tau_q)$ with

$$f(\tau_q) = \begin{cases} \arcsin^2\left(\frac{1}{\sqrt{\tau_q}}\right) & \tau_q \geq 1, \\ -\frac{1}{4}\left[\log\frac{1+\sqrt{1-\tau_q}}{1-\sqrt{1-\tau_q}} - i\pi\right]^2 & \tau_q < 1. \end{cases} \tag{2.5}$$

The analytical expression for $F_\square$ is too lenghty to present here and can be found in [14, 15].

The Higgs coefficients are:

$$C_\triangle = \frac{\lambda_{3H} v}{\hat{s} - m_H^2}, \; C_\square = 1. \tag{2.6}$$

After series expansion of the first term in eq. (2.5), $f(\tau_q)$ can be written as

$$f(\tau_q) = \frac{1}{\tau_q} + \frac{1}{3\tau_q^2} + \mathcal{O}\left(\left(\frac{\hat{s}}{4m_q^2}\right)^3\right). \tag{2.7}$$

In the infinite top mass approximation, $\tau_q \to +\infty$ and $F_\triangle$ becomes

$$F_\triangle^{EFT} = 2/3, \tag{2.8}$$

while [15]

$$F_\square^{EFT} = -2/3. \tag{2.9}$$

The comparison between EFT and the exact expression for the box MES we leave for future study. The expression in (2.3) reduces to:

$$\left|F_\triangle^{EFT} C_\triangle + F_\square^{EFT} C_\square\right|^2 = (2/3)^2 \left(\frac{\lambda_{3H}^2 v^2}{(\hat{s} - M_H)^2} - \frac{2\lambda_{3H} v}{\hat{s} - M_H} + 1\right). \tag{2.10}$$

In Fig. 2 the behaviour of $|C_\triangle F_\triangle^{EFT}|^2$ (dashed line), $|C_\square F_\square^{EFT}|^2$ (dotted line), $|C_\triangle F_\triangle^{EFT} + C_\square F_\square^{EFT}|^2$ (solid line) as a function of $\sqrt{\hat{s}}$ is displayed. In addition, $|C_\triangle F_\triangle|^2$ (dot-dashed line) is depicted. The genuine self-coupling contribution is only important for $\sqrt{\hat{s}}$ smaller than 400 GeV. The box contribution however, dominates over almost the full range for $\sqrt{\hat{s}}$. Near $\sqrt{\hat{s}} \simeq 2 \times m_H$ the interference between the triangle and box leads to sizeable cancellations. The figure also demonstrates that there is a large discrepancy between exact and approximate calculations of the triangle contribution for $\sqrt{\hat{s}} \gg 2m_q$. The triangle contribution to the MES contains the intermediate Higgs propagator, which is probed far off-shell at $\sqrt{\hat{s}} \gg m_H$. Therefore, this contribution becomes much smaller than the box, in which this propagator is absent. For increasing m_q in eqs. (2.4) and (2.5) the agreement between EFT and exact for the triangle improves.

We focus on the kinematical region $\sqrt{\hat{s}} < 2m_H$ as we expect that the triangle contribution dominates at these low energies. At $\sqrt{\hat{s}} < 2m_H$ the final state Higgses can no longer be both on-shell and the expression for the MES in eq. (2.3) is no longer valid. To cover the range where one or both final state Higgs bosons are off-shell we force one Higgs to decay

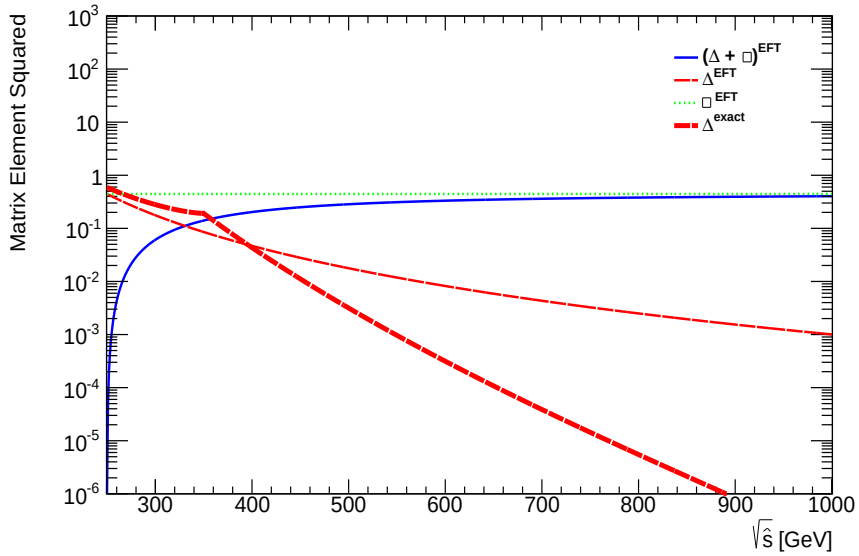

Figure 2. Comparison between: $\triangle^{EFT} \equiv |C_\triangle F_\triangle^{EFT}|^2$ (red-dashed), $\square^{EFT} \equiv |C_\square F_\square^{EFT}|^2$ (green-dotted), $(\triangle + \square)^{EFT} \equiv |C_\triangle F_\triangle^{EFT} + C_\square F_\square^{EFT}|^2$ (blue-solid), $\triangle^{\text{exact}} \equiv |C_\triangle F_\triangle|^2$ (thick red-dot-dashed).

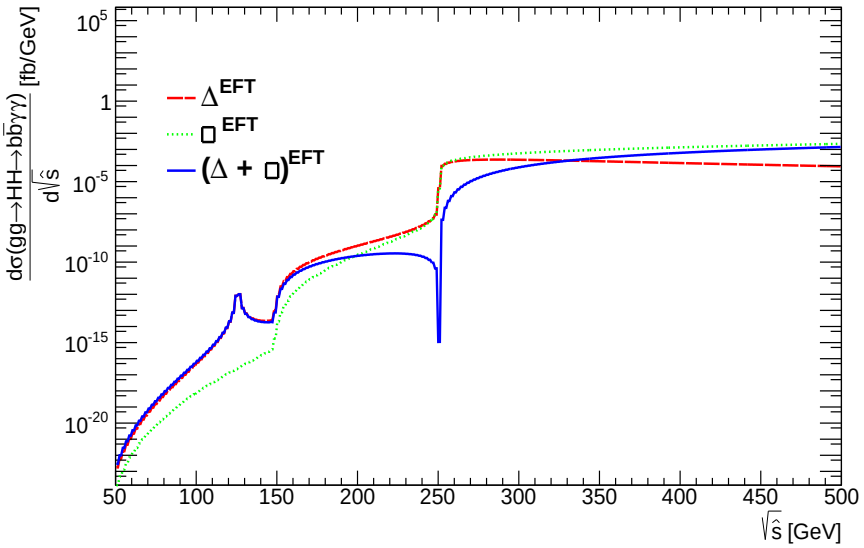

Figure 3. The $gg \to H^0H^0 \to b\bar{b}\gamma\gamma$ cross-section as a function of $\sqrt{\hat{s}}$. The results are obtained using Madgraph5 (EFT) [16]. Red-dashed line – 'triangle' only contribution, green-dotted line – only 'box' contribution, Blue-solid line – full result.

into $b\bar{b}$ and the other into $\gamma\gamma$. We analyse the behaviour of the partonic cross-section for $gg \to H^0H^0 \to b\bar{b}\gamma\gamma$ numerically with Madgraph5 [16] (EFT). The various contributions to this process, as a function of $\sqrt{\hat{s}}$, are shown in Fig. 3. The choice of decay modes affects

the total normalisation but not the shape of the distributions. The following cuts are used to ensure that the result is free from phase space singularities:

- pseudorapidity for each final state particle: $|\eta| < 2.5$,
- transverse momentum of each final state particle: $p_T > 10$ GeV,
- spatial separation: $\Delta R(b\bar{b}), \Delta R(b\gamma), \Delta R(\bar{b}\gamma), \Delta R(\gamma\gamma) > 0.4$,

where $\Delta R = \sqrt{(\Delta\phi)^2 + (\Delta\eta)^2}$, $\Delta\phi$ is the angle between two particles in the plane perpendicular to the incoming gluons and $\Delta\eta$ the difference in pseudorapidity. The region below $\sqrt{\hat{s}} = 125$ GeV in Fig. 3 corresponds to all Higgs bosons being off-shell, in the intermediate region 125 GeV $< \sqrt{\hat{s}} < 250$ GeV at least one Higgs is allowed to be on-shell. Obviously, above 250 GeV both favour to be on-shell. Due to the narrow Higgs width both the one and the two Higgs resonances appear as 'kinks'. In the vicinity of $\sqrt{\hat{s}}$ =125 GeV the rise of the total partonic cross-section is the result of the large influence of the Higgs propagator, as the triangle dominates. Close to $\sqrt{\hat{s}}$ =250 GeV, on the other hand, the box contribution is equally important. The partonic cross-section drops due to strong negative interference. Another 'kink' appears near $\sqrt{\hat{s}} = 145$ GeV. This is the result of the cut on the transverse momenta of the b-quarks and photons. In conclusion, only for the region $\sqrt{\hat{s}} < 200$ GeV the partonic cross-section is dominated by the contribution from the trilinear coupling. This unfortunately implies that the trilinear Higgs coupling adds only a small fraction to the total cross-section.

3 Higgs pair differential cross-section

In the following we convolute MES with gluon density functions (CTEQ6l [17]) and compare the leading order Higgs pair production cross-section $\sigma(pp \to H^0H^0)$ for exact and EFT calculations. For both we set the factorisation scale equal to the renormalisation scale ($\sqrt{\hat{s}}$).

In Fig. 4 we present two sets of curves. One set is obtained using EFT approximation (thin lines), the other set is the result of the exact approach (thick lines). Each set displays the differential cross-section for the triangle (dashed-dotted line) and box (dotted line) diagrams, and their sum (solid line). The exact calculations are obtained using [18]. We adapted Madgraph5[1] [16] to perform the EFT calculations. Despite the steep rise of the gluon density at small values of x, the cross-section below $\sqrt{\hat{s}} = 250$ GeV is negligible. At $\sqrt{\hat{s}} = 400$ GeV the exact calculation exceeds the EFT approximation for all cases. We find a large discrepancy between exact approach and EFT. The total cross-section at $\sqrt{\hat{s}} < 400$ GeV is dominated by the interference between triangle and box which, leads to large cancellations at $\sqrt{\hat{s}} = 2 \times m_H = 250$ GeV. Above this threshold the box dominates. The largest difference between exact and EFT appears for the the box only case. As a consequence, the total cross-section in EFT is underestimated at low and overestimated at high $\sqrt{\hat{s}}$. The triangle contribution in both exact and EFT is similar. EFT does not

[1]The EFT model in Madgraph5 does not include the ggHH coupling which, we implemented using Feynman rules given in [10]. Since each vertex is introduced separately, we obtain individual contributions for the triangle and box diagrams by forcing either of the couplings ggH=0 or ggHH=0.

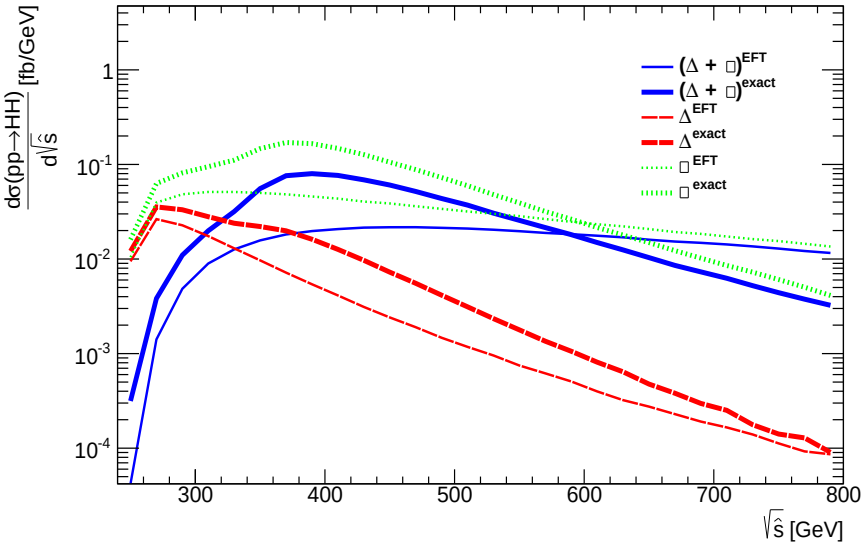

Figure 4. The differential Higgs pair production cross-section at leading order for the triangle, box, and both diagrams (including their interference). All contributions are obtained using both EFT and exact calculations (see legend).

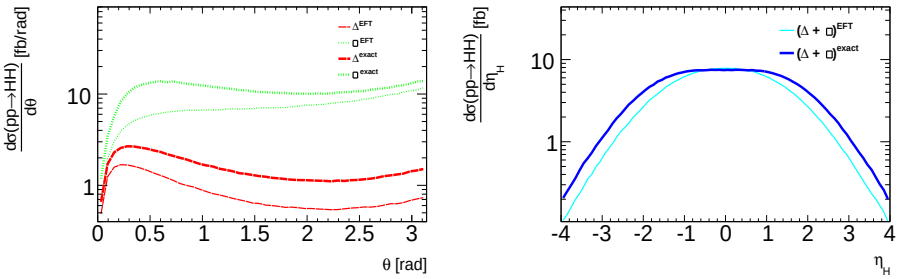

Figure 5. Left plot: comparison between the distributions of the opening angle between the two Higgs momenta in EFT (thin lines) and exact calculation (thick lines) for the triangle (red lines) and box (green lines). Right plot: Comparison between the inclusive Higgs pseudorapidity distributions for EFT (thin light line) and exact (thick dark line) calculation.

reproduce the kink at $2 \times m_q$ (which is the result of using the approximate form factor of eq. (2.8) instead of the one in eqs. (2.4) and (2.5), see Fig. 2). In the left plot in Fig. 5 we compare the angle between the two Higgses in the laboratory frame (exact– thick lines, EFT– thin lines) for the box (dotted) and triangle (dashed-dotted) contributions. For the triangle, both approaches give similar shapes. For the box, the difference between exact and EFT calculations decreases when the Higgses get more back-to-back. The exact calculations show a larger preference for the two Higgses to have a small opening angle. This effect is less pronounced in the EFT calculations and can be explained by analysing the right graph in Fig. 5. Here, the rapidity of each Higgs is presented. Loop calculations result in a broader distribution which, is caused by larger differences between the Bjorken x of the colliding

gluons. As a result, the di-Higgs system receives a larger longitudinal boost despite lower mean value of $\sqrt{\hat{s}}$. In conclusion; EFT calculations do not represent the kinematics of Higgs pair production. This is due to oversimplification of the – dominant – box contribution.

4 Disentangling the signal from irreducible background

The discussion in the previous section demonstrates that the kinematical region in which Higgs pair production cross-section is most sensitive to the self-coupling contribution, is where $\sqrt{\hat{s}} < 400$ GeV. Next, we will examine how this energy dependence affects kinematical properties of the decay products of both Higgses. We exclude EFT calculations of the signal and study only exact distributions.

In Table 2 the event yields for $b\bar{b}b\bar{b}$, $b\bar{b}W^+W^-$, $b\bar{b}Z^0Z^0$, $b\bar{b}\gamma\gamma$, and 4γ final states are given. We compare three variants: 8 TeV with an integrated luminosity of 20 fb^{-1} (as collected by the ATLAS and CMS experiments during the LHC Run I), High Luminosity LHC with 3000 fb^{-1} at 14 TeV, and 3000 fb^{-1} at a 100 TeV hadron collider. The numbers are based on Higgs pair production cross-sections at LO and NLO [10] taking into account the proper Higgs branching ratios [12]. Except for both Higgses decaying into bottom quarks, the choice of these channels is motivated by the observation of the (single) Higgs decay into $\gamma\gamma$, Z^0Z^0 and W^+W^- by the ATLAS and CMS collaborations [3, 4]. The 4γ channel suffers from lack of statistics and will therefore be ignored in our analyses. One might argue, however, that this final state poses a real challenge at a 100 TeV hadron collider (21 events). To provide sufficient statistics at the HL-LHC, at least one Higgs decay should have a large branching ratio, for instance $b\bar{b}$ or $\tau^+\tau^-$. The $b\bar{b}b\bar{b}$, $b\bar{b}W^+W^-$ and $b\bar{b}Z^0Z^0$ channels suffer from large backgrounds. The $b\bar{b}\gamma\gamma$ final state compromises between reasonable statistics and a relatively clean experimental signature. We examine whether this signal can be distinguished from irreducible $b\bar{b}\gamma\gamma$ backgrounds resulting from QCD, QED and single Higgs production ($Z^0H(\gamma\gamma)$, $b\bar{b}H(\gamma\gamma)$).

We study $pp \to HH \to b\bar{b}\gamma\gamma$ neglecting initial and final state radiation. Moreover, we do not take into account possible dilution effects due to reconstruction inefficiencies or mis-reconstruction. Thus we exclude other (reducible) backgrounds containing for instance two photons and two light quark jets, top anti-top pairs, top anti-top pairs with single photons, and top anti-top pairs with Higgses decaying into two photons. There have been several phenomenological studies on the $b\bar{b}\gamma\gamma$ channel, see for instance [13, 19, 20]. We take a different approach and analyse the box and triangle contributions separately in order to find kinematical regions in which the sensitivity to the trilinear coupling is largest. We also discuss the feasibility of separating the genuine self-coupling from the irreducible background. We apply the following cuts to our $b\bar{b}\gamma\gamma$ samples [19]:

$$\begin{aligned} &p_T(b) > 45 \text{ GeV},\ |\eta(b)| < 2.5,\ \Delta R(b,b) > 0.4, \\ &p_T(\gamma) > 20 \text{ GeV},\ |\eta(\gamma)| < 2.5,\ \Delta R(\gamma,\gamma) > 0.4, \end{aligned} \tag{4.1}$$

and

$$|m_{bb} - m_H| < 20 \text{ GeV}, |m_{\gamma\gamma} - m_H| < 2.3 \text{ GeV}. \tag{4.2}$$

HH final state	Br. Rat.	8 TeV(20 fb^{-1}) LO (NLO)	14 TeV (3000 fb^{-1}) LO (NLO)	100 TeV (3000 fb^{-1}) LO (NLO)
$b\bar{b}b\bar{b}$	32.5%	23 (60)	16×10^3 (33×10^3)	0.85×10^6 (1.3×10^6)
$b\bar{b}W^+W^-$	23.9%	17 (44)	12×10^3 (24×10^3)	0.63×10^6 (0.97×10^6)
$b\bar{b}Z^0Z^0$	3.0%	2.2 (5.5)	1.5×10^3 (3×10^3)	0.08×10^6 (0.12×10^6)
$b\bar{b}\gamma\gamma$	0.26%	0.19 (0.48)	128 (264)	6800 (10500)
$\gamma\gamma\gamma\gamma$	0.001%	0 (0)	0.25 (0.53)	14 (21)

Table 2. Expected event yields for di-Higgs production form gluon fusion and different di-Higgs decay channels, based on the LO [18] (NLO [10]) Higgs pair production cross section: 3.58 (9.22) fb, 16.23 (33.86) fb, and 877 (1350) fb at 8, 14, and 100 TeV, respectively.

The cuts on transverse momentum and rapidity are motivated by trigger capabilities and detector coverage. The rather tight cuts on invariant masses increase the signal to background ratio.

In Fig. 6 the ΔR separation between the two photons (upper plot) and between the photon and the b ($\bar{b}$) quark that are closest in phase space (lower plot) are displayed. The individual distributions for the full cross-section (solid line), the genuine self-coupling contribution (dashed line), and $b\bar{b}\gamma\gamma$ background (dotted line) are presented. The background processes containing single Higgses are calculated using EFT [16]. The distribution of ΔR between photons for the Higgs pair reaches a maximum at $\Delta R(\gamma,\gamma) \simeq 1.5$ due to the large boost of the di-Higgs system. It is well separated from the background, in which the two photons do not stem from the same parent. The kinematical properties of the triangle and triangle+box samples are different due to the domination of the box. The former favours $\Delta R(\gamma\gamma) \simeq 3$ while the latter has a maximum for small values of ΔR. The minimum separation between a photon and a b ($\bar{b}$) quark in the background sample is small as most photons are emitted from the quarks and hence prefer to be collinear with their parents. In our two di-Higgs samples on the other hand, these particles are the Higgs decay products and are much more separated. The relatively large contribution from the box increases this separation.

Fig. 6 leads to the conclusion that it is extremally challenging to isolate the genuine self-coupling contribution from the irreducible background. Different shapes of the overall SM di-Higgs production and the trilinear coupling contribution suggest that the strategy optimised to isolate the former might not be best for enhancing the sensitivity to the latter. We will discuss this issue more quantitatively in the following section.

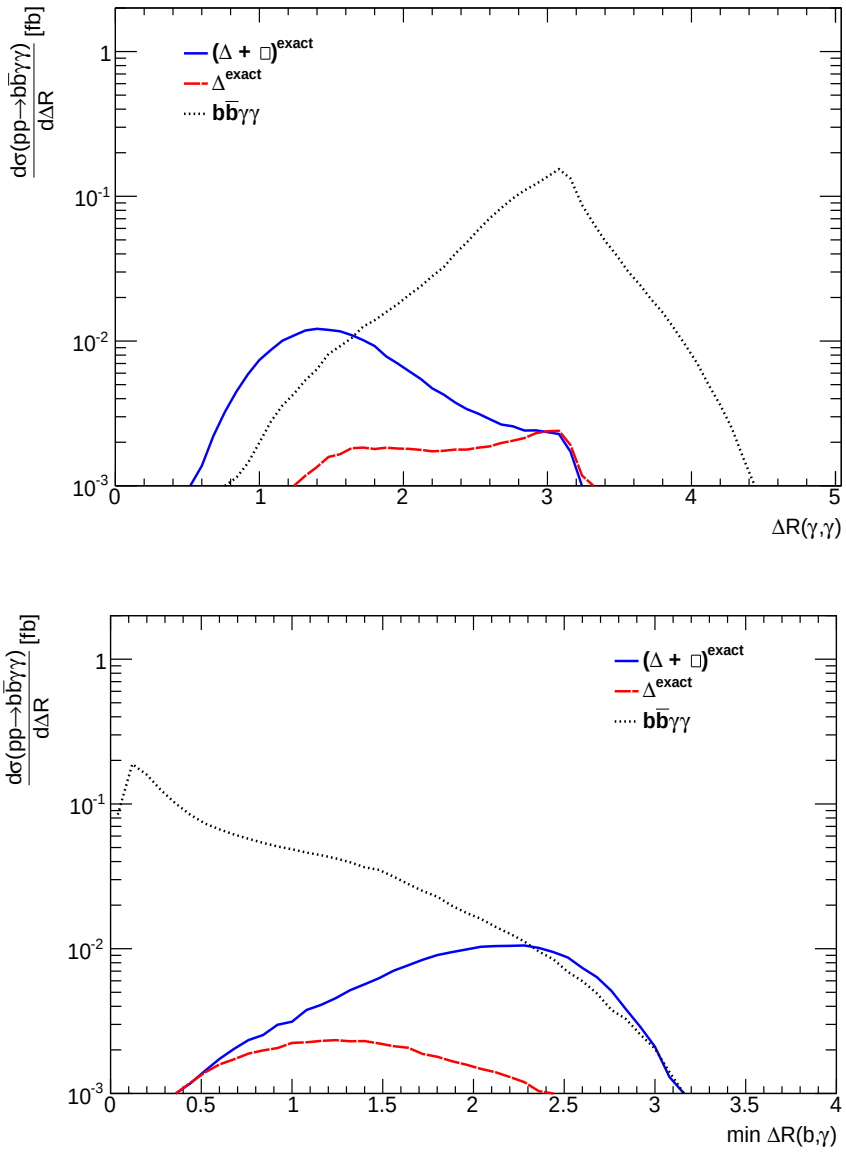

Figure 6. The distributions of $\Delta R(\gamma,\gamma)$ (upper plot) and $\Delta R(b,\gamma)_{\rm min}$ (lower plot) for the SM Higgs pair production (blue-solid line), the triangle contribution separately (red-dashed line) and the irreducible $b\bar{b}\gamma\gamma$ background (black-dotted line).

5 Non Standard Model values of λ_{3H}

If the magnitude of the Higgs self-coupling is not in accordance with its SM value, the electroweak symmetry breaking is not, or only in part, a result of the SM Higgs potential of eq. (1.1). As a consequence, m_H, VEV and λ_{3H} in eq. (1.3) are decoupled and the observed 125 GeV resonance is not the SM Higgs. It may instead be a member of a more extended sector (see for instance [21]) or be composite and strongly interacting [22, 23].

We study how the kinematics in Higgs pair production changes assuming the trilinear

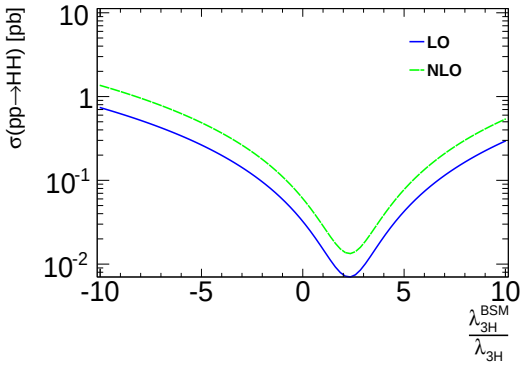

Figure 7. Di-Higgs cross-sections at $\sqrt{s} = 14$ TeV for different values of λ_{3H}^{BSM}, obtained using [10, 15].

Higgs coupling is a free parameter. We do not focus on any model in particular and therefore do not modify any other SM parameter. In the following λ_{3H}^{BSM} denotes the BSM value. The triangle contribution to the cross-section changes quadratically with λ_{3H}^{BSM}, while the triangle-box interference shows a linear dependence. For $\lambda_{3H}^{BSM} < 0$ the interference term flips sign and the cross-section becomes larger than for corresponding positive λ_{3H}^{BSM}. This behaviour is depicted in Fig. 7 showing the di-Higgs cross-section at $\sqrt{s} = 14$ TeV at LO (solid line) and NLO (dashed line)[2] as a function of $\lambda_{3H}^{BSM}/\lambda_{3H}$. Note that for $\lambda_{3H}^{BSM} = 0$ only the box contributes and the cross-section is larger than for $\lambda_{3H}^{BSM} = \lambda_{3H}$. To quantitatively determine the size of the individual contributions we compare LO cross-sections for $\lambda_{3H}^{BSM} = \lambda_{3H}, 0$ and $-\lambda_{3H}$. We find that $\sigma^{\square} \simeq 35$ fb, $\sigma^{int} \simeq -25$ fb, $\sigma^{\triangle} \simeq 5$ fb, while the total SM cross-section $\simeq 17$ fb. Due to the large box contribution the sensitivity of the total cross-section to λ_{3H}^{BSM} is small[3]. Fig. 7 shows large differences between LO and NLO. The NLO K-factor ($\equiv \sigma^{NLO}/\sigma^{LO}$) is displayed in Fig. 8 (left) as a function of λ_{3H}^{BSM}. For $\lambda_{3H}^{BSM} = \lambda_{3H}$ the K-factor becomes rather large $\simeq$1.92 [4] (see Table 2). It slightly dependends on λ_{3H}^{BSM} due to different QCD corrections to box and triangle contributions. In the right plot in Fig. 8 the K-factors at $\sqrt{s} = 14$ TeV and 100 TeV are compared. As expected, the role of NLO corrections is smaller at higher $\sqrt{s}$. The absolute value of the di-Higgs cross-section at 100 TeV is over a factor of 100 larger than at 14 TeV (see Table 2). The sensitivity to different values of λ_{3H}^{BSM} is, however, smaller.

Fig. 9 presents the differential cross-sections for the processes $pp \to HH \to b\bar{b}\gamma\gamma$ and $pp \to b\bar{b}\gamma\gamma$ after applying the cuts of eqs. (4.1) and (4.2). The SM Higgs pair production is displayed as solid line, the genuine self-coupling as dashed, BSM Higgs pair production with $\lambda_{3H}^{BSM} = 10\lambda_{3H}$ as dotted, and irreducible $b\bar{b}\gamma\gamma$ background as dashed-dotted line. We focus on BSM with $\lambda_{3H}^{BSM} = 10\lambda_{3H}$. The BSM cross-section is approximately 60 times

[2] At NLO the Born term was computed with exact quark loop and the QCD corrections were included in EFT approximation. Both LO and NLO were obtained with [10].

[3] The sensitivity of different di-Higgs production channels to different values of λ_{3H}^{BSM} can be found in ref. [13].

[4] This value is larger than quoted in [10] (1.92 instead of 1.86) as we used a more recent set of PDFs.

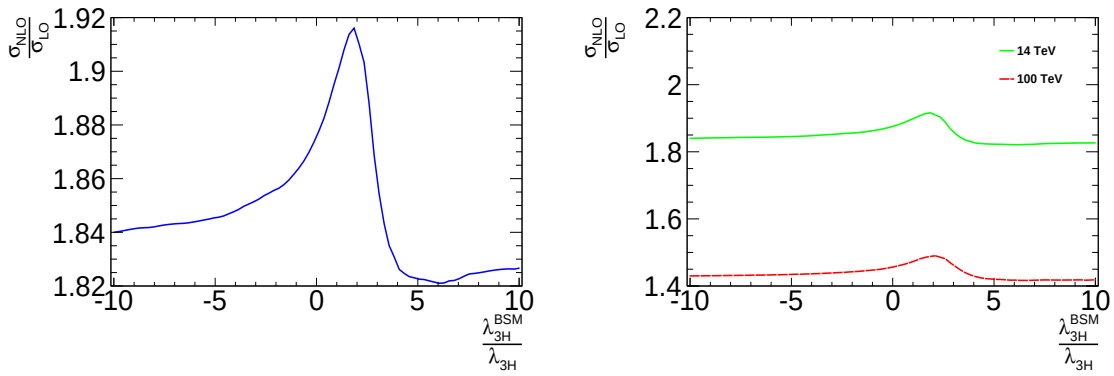

Figure 8. NLO K factors as a function of λ_{3H}^{BSM} from HPAIR with CTEQ6 [24] at $\sqrt{s} = 14$ TeV (left plot) and for $\sqrt{s} = 14$ and 100 TeV (right plot).

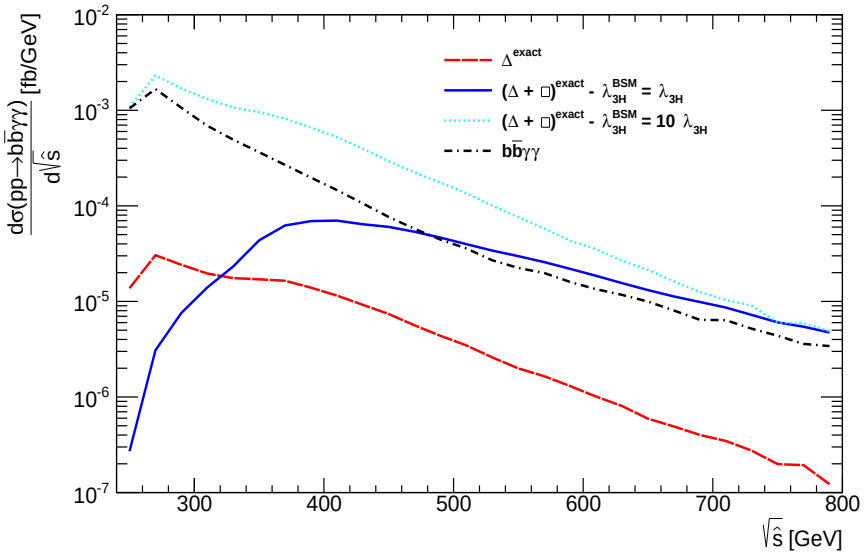

Figure 9. The differential di-Higgs production cross-section for $\lambda_{3H}^{BSM} = \lambda_{3H}$ (dark blue-dashed line), $\lambda_{3H}^{BSM} = 10\lambda_{3H}$ (light blue-dotted line) and genuine self-interactions (red-solid line) and $b\bar{b}\gamma\gamma$ background differential cross-section (black dash-dotted line). The cuts of eq. (4.1) and (4.2) are applied.

larger than that of the pure triangle and two times larger than the irreducible background, reaches the maximum at $\sqrt{\hat{s}} = 270$ GeV and decreases exponentially for large $\sqrt{\hat{s}}$. Unlike the SM cross-section at $\sqrt{\hat{s}} < 400$ GeV, at large values of λ_{3H}^{BSM} the cancelations due to negative interference are negligible. On the other hand, at $\sqrt{\hat{s}} > 750$ GeV SM and BSM cross-sections become about equal as all sensitivity to Higgs trilinear coupling is lost.

In Fig. 10 we compare ΔR distributions for the SM and BSM Higgs pair production mechanisms, and for the irreducible background. The dashed line corresponds to $\lambda_{3H}^{BSM} = 10\lambda_{3H}$, dash-dotted line to $\lambda_{3H}^{BSM} = 0$, solid line to the SM and dotted line to the $b\bar{b}\gamma\gamma$

Cuts	B	$S(\lambda_{3H})$	$S(10\times\lambda_{3H})$	$S(\lambda_{3H})/\sqrt{B}$	$S(10\times\lambda_{3H})/\sqrt{B}$
Before cuts	–	128	2280	–	–
eq. (4.1)	166950	48	726	0.12	1.78
eq. (4.2)	395	48	726	2.43	36.53
eq.(5.1a)	26	35	189	6.80	36.85
eq.(5.1b)	41	39	256	6.10	40.16
eq.(5.1c)	240	48	679	3.08	43.84

Table 3. The number of events in: $b\bar{b}\gamma\gamma$ background, SM and BSM with $\lambda_{3H}^{BSM}=10\lambda_{3H}$ predicted for the luminosity upgraded LHC ($\mathcal{L}=3000\text{fb}^{-1}$).

background. As the triangle dominates at small $\sqrt{\hat{s}}$ mean separation between the two photons (upper plot) is larger for $\lambda_{3H}^{BSM}=10\lambda_{3H}$ than for $\lambda_{3H}=0$. The shape of the pure box sample resembles the SM and its larger cross-section is due to the absence of negative interference. The minimum separation $\Delta R(b,\gamma)$ (upper plot) is on average smaller for $\lambda_{3H}^{BSM}=10\lambda_{3H}$ than for pure box. The larger cross-section for $\lambda_{3H}^{BSM}=10\lambda_{3H}$ with $\Delta R(b,\gamma)>0.4$ on the other hand, separates the triangle from the kinematically similar background. For $\lambda_{3H}=0$ the signal exceeds the background for $\Delta R(b,\gamma)>2$. We proceed with three variants of ΔR cuts:

$$\Delta R(\gamma,\gamma)<2,\quad \Delta R(b,\gamma)>1.0; \tag{5.1a}$$

$$\Delta R(\gamma,\gamma)<2.2,\quad \Delta R(b,\gamma)>0.4; \tag{5.1b}$$

$$\text{no cut on } \Delta R(\gamma,\gamma),\quad \Delta R(b,\gamma)>0.4; \tag{5.1c}$$

with the aim to improve the separation as compared to the cuts presented in eq. (5.1a) (see ref. [19]), Table 3 shows the event yields after applying cuts. The background is generated with the cuts of eq. (4.1) excluding potential soft and collinear singularities. The invariant mass cuts of eq. (4.2) significantly reduce the background and retain the SM and BSM signal. $\Delta R(\gamma,\gamma)$ and $\Delta R(b,\gamma)$ must be chosen differently to optimise for SM and BSM. The cuts of eq. (5.1a) give the best results for SM di-Higgs production and are less efficient for large values of λ_{3H}^{BSM}. The cuts of eq. (5.1c) are optimised for $\lambda_{3H}^{BSM}=10\lambda_{3H}$.

6 Conclusions

In view of the upgrade of the LHC to reach higher luminosities it is vital to study the production and observability of pairs of Higgs bosons and how to measure their self-couplings. We investigated the trilinear coupling in Higgs pair production in gluon fusion with the Higgs bosons decaying into $b\bar{b}\gamma\gamma$. With the LHC data collected at 8 TeV ($\mathcal{L}\simeq 20$ fb^{-1}) we envisage 0.5 signal events (Table 2) before experimental reconstruction. Recently, the ATLAS collaboration presented the results of a search for Higgs pairs in their dataset [25]. They observe an excess of di-Higgs candidates with a significance of $\sim 2\sigma$.

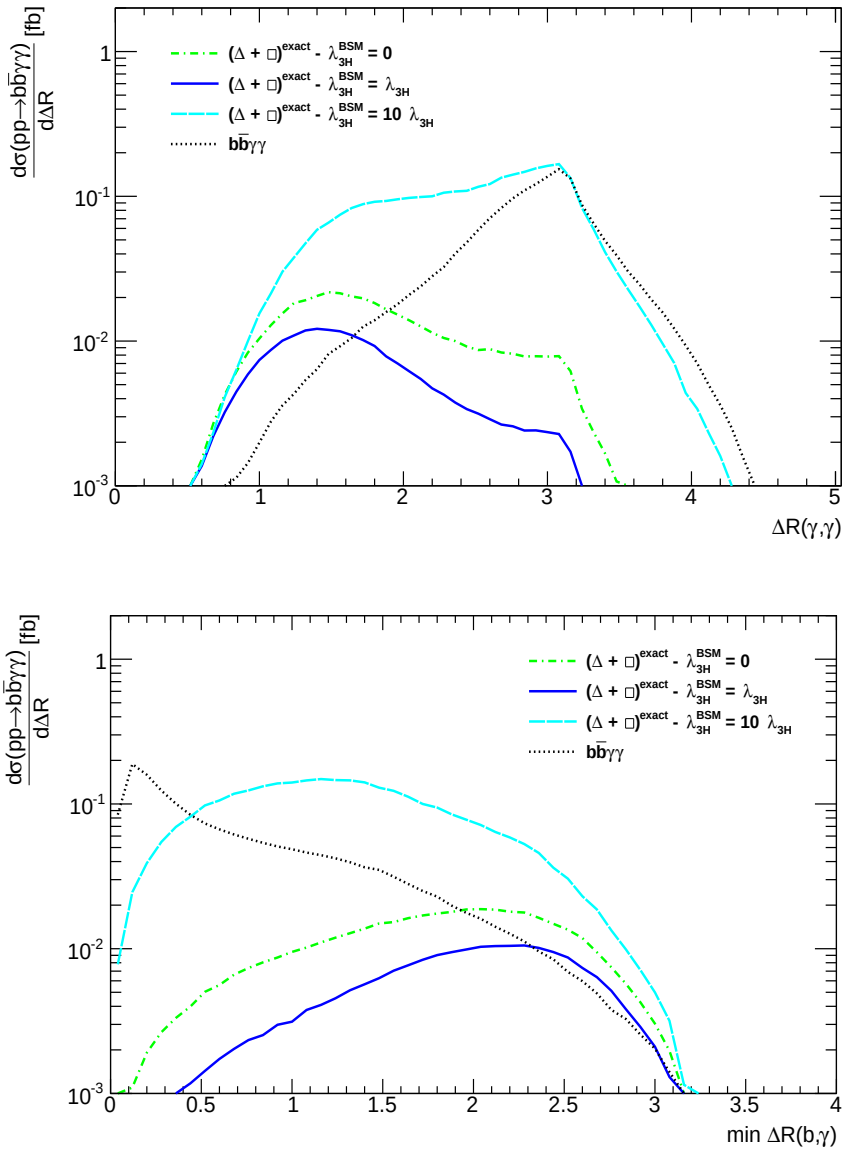

Figure 10. $\Delta R(\gamma,\gamma)$ (upper plot) and $\Delta R(b,\gamma)_{\min}$ (lower plot) for SM di-Higgs production (dark blue-solid line), BSM with $\lambda_{3H}^{BSM} = 10\lambda_{3H}$ (dark blue-dashed line), BSM with $\lambda_{3H}^{BSM} = 0$ (green dash-dotted line) and irreducible background (black-dotted line). The cuts of eqs. (4.1) and (4.2) have been applied.

As the di-Higgs cross-section is small, detailed knowledge on the kinematics is required to improve the separation between signal and irreducible background. Several cross-section predictions in the literature exploit EFT approximation at leading [26] or higher orders [10, 11, 13]. We confronted EFT with an exact matrix element calculation at leading order. At $\sqrt{\hat{s}} \simeq 2m_q$ we find large differences. EFT neglects part of the complicated structure of the box MES which, adds significantly to the discrepancy due to the triangle contribution. For

the exact calculation we obtain a larger longitudinal boost for and an on average smaller opening angle between the Higgs bosons, in agreement with previous studies [27–29].

To get a better understanding of how the triangle and box contribute to the MES, we studied their behaviour over a large interval of $\sqrt{\hat{s}}$. We show that the phase space region in which the relative contribution of the self-coupling maximises is around $\sqrt{\hat{s}} \simeq m_H$. The contribution to the MES in this region is, however, very small. At large values of $\sqrt{\hat{s}}$ the trilinear coupling plays no role anymore. This is in agreement with the observations presented in [20]. For a non-negligible contribution from the trilinear Higgs coupling, experimental searches should focus on the region where $\sqrt{\hat{s}} < 400$ GeV.

We modified the kinematical cuts proposed in ref. [19] to study the $b\bar{b}\gamma\gamma$ final state. They provide a good separation between di-Higgs signal and irreducible background. To determine if additional selection criteria should improve the λ_{3H} measurement, we increased λ_{3H} by a factor of 10. This leads to the cuts in (5.1c).

Acknowledgments

We would like to thank Michael Spira and Marco Zaro for help in using their programs. M.S. acknowledges a useful discussion with Tilman Plehn.

References

[1] **ATLAS** Collaboration, G. Aad *et. al.*, *Observation of a new particle in the search for the Standard Model Higgs boson with the ATLAS detector at the LHC*, *Phys.Lett.* **B716** (2012) 1–29, [arXiv:1207.7214].

[2] **CMS** Collaboration, S. Chatrchyan *et. al.*, *Observation of a new boson at a mass of 125 GeV with the CMS experiment at the LHC*, *Phys.Lett.* **B716** (2012) 30–61, [arXiv:1207.7235].

[3] **ATLAS** Collaboration *ATLAS-CONF-2013-013,ATLAS-CONF-2013-030, ATLAS-CONF-2013-031* (2013).

[4] **CMS** Collaboration *CMS-PAS-HIG-13-001, CMS-PAS-HIG-13-002, CMS-PAS-HIG-13-003* (2013).

[5] F. Englert and R. Brout, *Broken Symmetry and the Mass of Gauge Vector Mesons*, *Phys.Rev.Lett.* **13** (1964) 321–323.

[6] P. W. Higgs, *Broken Symmetries and the Masses of Gauge Bosons*, *Phys.Rev.Lett.* **13** (1964) 508–509.

[7] A. Djouadi, M. Spira, and P. Zerwas, *Production of Higgs bosons in proton colliders: QCD corrections*, *Phys.Lett.* **B264** (1991) 440–446.

[8] M. Spira, A. Djouadi, D. Graudenz, and P. Zerwas, *Higgs boson production at the LHC*, *Nucl.Phys.* **B453** (1995) 17–82, [hep-ph/9504378].

[9] S. Dawson, *Radiative corrections to Higgs boson production*, *Nucl.Phys.* **B359** (1991) 283–300.

[10] S. Dawson, S. Dittmaier, and M. Spira, *Neutral Higgs boson pair production at hadron colliders: QCD corrections*, *Phys.Rev.* **D58** (1998) 115012, [hep-ph/9805244].

[11] D. de Florian and J. Mazzitelli, *Higgs Boson Pair Production at Next-to-Next-to-Leading Order in QCD*, *Phys. Rev. Lett. 111,* **201801** (2013) 201801, [arXiv:1309.6594].

[12] **LHC Higgs Cross Section Working Group** Collaboration, S. Dittmaier *et. al.*, *Handbook of LHC Higgs Cross Sections: 1. Inclusive Observables*, arXiv:1101.0593.

[13] J. Baglio, A. Djouadi, R. Gröber, M. Mühlleitner, J. Quevillon, *et. al.*, *The measurement of the Higgs self-coupling at the LHC: theoretical status*, *JHEP* **1304** (2013) 151, [arXiv:1212.5581].

[14] E. N. Glover and J. van der Bij, *Higgs boson pair production via gluon fusion*, *Nucl.Phys.* **B309** (1988) 282.

[15] T. Plehn, M. Spira, and P. Zerwas, *Pair production of neutral Higgs particles in gluon-gluon collisions*, *Nucl.Phys.* **B479** (1996) 46–64, [hep-ph/9603205].

[16] J. Alwall, R. Frederix, S. Frixione, V. Hirschi, F. Maltoni, *et. al.*, *The automated computation of tree-level and next-to-leading order differential cross sections, and their matching to parton shower simulations*, *JHEP* **1407** (2014) 079, [arXiv:1405.0301].

[17] J. Pumplin, D. Stump, J. Huston, H. Lai, P. M. Nadolsky, *et. al.*, *New generation of parton distributions with uncertainties from global QCD analysis*, *JHEP* **0207** (2002) 012, [hep-ph/0201195].

[18] R. Frederix, S. Frixione, V. Hirschi, F. Maltoni, O. Mattelaer, *et. al.*, *Higgs pair production at the LHC with NLO and parton-shower effects*, *Phys.Lett.* **B732** (2014) 142–149, [arXiv:1401.7340]. Code available from https://cp3.irmp.ucl.ac.be/projects/madgraph/attachment/wiki/HiggsPairProduction/SM.tar.gz.

[19] U. Baur, T. Plehn, and D. L. Rainwater, *Probing the Higgs selfcoupling at hadron colliders using rare decays*, *Phys.Rev.* **D69** (2004) 053004, [hep-ph/0310056].

[20] M. J. Dolan, C. Englert, and M. Spannowsky, *Higgs self-coupling measurements at the LHC*, *JHEP* **1210** (2012) 112, [arXiv:1206.5001].

[21] H. Georgi and M. Machacek, *DOUBLY CHARGED HIGGS BOSONS*, *Nucl.Phys.* **B262** (1985) 463.

[22] G. Giudice, C. Grojean, A. Pomarol, and R. Rattazzi, *The Strongly-Interacting Light Higgs*, *JHEP* **0706** (2007) 045, [hep-ph/0703164].

[23] R. Grober and M. Muhlleitner, *Composite Higgs Boson Pair Production at the LHC*, *JHEP* **1106** (2011) 020, [arXiv:1012.1562].

[24] S. Kretzer, H. Lai, F. Olness, and W. Tung, *Cteq6 parton distributions with heavy quark mass effects*, *Phys.Rev.* **D69** (2004) 114005, [hep-ph/0307022].

[25] **ATLAS** Collaboration, G. Aad *et. al.*, *Search For Higgs Boson Pair Production in the gamma gamma b bbar Final State using pp Collision Data at sqrt(s)=8 TeV from the ATLAS Detector*, arXiv:1406.5053.

[26] J. Alwall, M. Herquet, F. Maltoni, O. Mattelaer, and T. Stelzer, *MadGraph 5 : Going Beyond*, *JHEP* **1106** (2011) 128, [arXiv:1106.0522].

[27] S. Dawson, E. Furlan, and I. Lewis, *Unravelling an extended quark sector through multiple Higgs production?*, *Phys.Rev.* **D87** (2013) 014007, [arXiv:1210.6663].

[28] Q. Li, Q.-S. Yan, and X. Zhao, *Higgs Pair Production: Improved Description by Matrix Element Matching*, *Phys.Rev.* **D89** (2014) 033015, [arXiv:1312.3830].

[29] J. Grigo, J. Hoff, K. Melnikov, and M. Steinhauser, *On the Higgs boson pair production at the LHC*, *Nucl.Phys.* **B875** (2013) 1–17, [arXiv:1305.7340].